Paleoceanography and Paleoclimatology

RESEARCH ARTICLE
10.1029/2019PA003731

Selective Preservation of Coccolith Calcite in Ontong-Java Plateau Sediments

Adam V. Subhas[1,2], Daniel C. McCorkle[3], Alex Quizon[4], Ann P. McNichol[2,3], and Matthew H. Long[1]

[1]Department of Marine Chemistry and Geochemistry, Woods Hole Oceanographic Institution, Woods Hole, MA, USA, [2]National Ocean Sciences Accelerator Mass Spectrometry Facility, Woods Hole, MA, USA, [3]Department of Geology and Geophysics, Woods Hole Oceanographic Institution, Woods Hole, MA, USA, [4]Department of Chemistry, Williams College, Williamstown, MA, USA

Key Points:
- Coccolith calcite is preferentially preserved in Ontong-Java Plateau sediments and foraminifera preferentially dissolved
- Preferential dissolution appears to be linked to Mg content
- Coccolith-foraminifera radiocarbon age offsets, on the order of 1,000 years, are a result of within-sediment dissolution

Supporting Information:
- Supporting Information S1
- Data Set S1
- Data Set S2

Correspondence to:
A. V. Subhas,
asubhas@whoi.edu

Citation:
Subhas, A. V., McCorkle, D. C., Quizon, A., McNichol, A. P., & Long, M. H. (2019). Selective preservation of coccolith calcite in Ontong-Java Plateau sediments. *Paleoceanography and Paleoclimatology*, *34*, 2141–2157. https://doi.org/10.1029/2019PA003731

Received 20 JUL 2019
Accepted 31 OCT 2019
Accepted article online 15 NOV 2019
Published online 26 DEC 2019

Abstract Dissolution of calcite in deep ocean sediments, which is required to balance global marine $CaCO_3$ production and burial fluxes, is still a poorly understood process. In order to assess the mechanisms of dissolution in sediments, we analyzed four multicore tops taken along a depth transect on the Ontong-Java Plateau. These cores were taken directly on the equator, and span water column calcite saturation states from ~0.93 to ~0.74, allowing us to assess the effect of dissolution on carbonate sediment composition. The top 2 cm of each multicore was sectioned and sieved to separate coccolith from foraminiferal calcite, and the $\%CaCO_3$, $\delta^{13}C$, $\Delta^{14}C$, and Mg/Ca were evaluated. The mass ratio of coccoliths to foraminifera increases by a factor of 3 as a function of water depth, reflecting the preferential dissolution of foraminifera. Carbon isotope ($\delta^{13}C$ and $\Delta^{14}C$) data suggest that most dissolution takes place at the sediment-water interface and primarily affects foraminifera. Mg/Ca analyses indicate that the Mg content of the entire foraminiferal assemblage decreases as a function of dissolution. In contrast, coccolith dissolution takes place within the sediments, rather than at the interface. Together these two processes cause coccoliths to be up to 1,000 radiocarbon years younger than foraminifera from the same depth horizon. Despite this within-sediment coccolith dissolution flux, sediments below the calcite saturation horizon remain enriched in coccolith calcite. Combined with global seafloor hypsometry and calcium carbonate content, this enrichment suggests that globally, coccoliths may outweigh foraminifera in deep ocean sediments by a factor of 1.8.

1. Introduction

The large reservoir of accumulated biogenic calcite in the deep ocean is responsible for setting the whole-ocean carbonate ion concentration and maintaining ocean alkalinity balance through time (Archer, 1996; Boudreau et al., 2018). Carbonate sediments also help neutralize anthropogenic CO_2 emissions into the ocean-atmosphere system, because carbonate dissolution buffers seawater as CO_2 is converted to bicarbonate (Archer et al., 1998; Sulpis et al., 2018). This neutralization reaction relies on the chemistry of seawater and properties of the calcite mineral itself.

It is clear that not all biogenic calcites are the same. Each species of foraminifera appears to incorporate a different amount of magnesium into its test, which is a function of both temperature and a species-specific magnesium incorporation factor (Anand et al., 2003). Likewise, the $\delta^{13}C$ of foraminiferal calcite relative to seawater must be calibrated for each species, suggesting interspecies differences in calcite biomineralization and chemical composition (Spero et al., 1997). These interspecies differences also point to mineralogical heterogeneity, which in turn could influence the relative susceptibility of foraminifera to dissolution. Planktic foraminiferal assemblages change as a function of dissolution, suggesting that some species are more resistant to dissolution (Adelseck, 1977; Le & Thunell, 1996; Parker & Berger, 1971; Thunell, 1976).

Foraminiferal tests are not the only form of calcite found in deep ocean sediments. Coccoliths and foraminifera are, on average, present in equal mass in sediments above the calcite saturation horizon (Broecker & Clark, 2009). In laboratory and field experiments, foraminiferal calcite dissolves faster than coccolith calcite (Honjo & Erez, 1978; Subhas et al., 2018). Some sediment core data also suggest that foraminifera are preferentially dissolved in sediments below the saturation horizon

Table 1
Locations of the four cores in this study

Core	Depth (km)	Latitude	Longitude	$\Omega_{calcite}$
MW97-20 MC55	2.767	−0°0.25′N	159°52.16′E	0.93
MW97-20 MC45	3.368	−0°0.22′N	160°59.31′E	0.85
MW97-20 MC39	3.705	−0°0.28′N	161°23.14′E	0.82
MW97-20 MC28	4.325	−0°0.22′N	162°13.28′E	0.74

Note. The upper 2 cm, sectioned in 0.5-cm intervals, were used from each core. Saturation state is shown from the closest water column profile with carbonate chemistry measurements (0.077°S, from the GLODAP v2.2019 database (Olsen et al., 2016, 2019).

(Chiu and Broecker, 2008). It is therefore possible that differences in the mineralogy of coccolith and foraminiferal calcite exert some level of control over where and how fast calcite dissolves in sediments. However, the relative distribution of coccoliths and foraminifera has not been systematically evaluated below the saturation horizon.

The radiocarbon age of bulk carbonate in surface sediments has helped to elucidate some of the mechanistic controls on dissolution. At many locations, surface sediments show increasing radiocarbon ages with water depth, implying that a significant portion of dissolution occurs at or above the sediment-water interface (Broecker et al., 1991, 1999; Oxburgh & Broecker, 1993; Oxburgh, 1998; Martin et al., 2000). Barker et al. (2007) also documented radiocarbon age offsets between planktic foraminiferal species and also between whole foraminiferal tests and their fragments. These age offsets imply a systematic, but currently unknown, relationship between residence time in the sedimentary mixed layer and foraminiferal dissolution. It is also possible that the distinct dissolution behavior of coccoliths and foraminifera results in coccolith-foraminifera radiocarbon age offsets.

Here, we combine mass, $\delta^{13}C$, $\Delta^{14}C$, and Mg/Ca data of size-fractionated Ontong-Java Plateau sedimentary carbonate to show dissolution trends of coccoliths and foraminifera as a function of water depth. We then develop a framework for understanding the relative dissolution susceptibility of foraminifera and coccoliths. Finally, we use these results in a calculation of calcite inventory and assess the relative contribution of coccoliths and foraminifera to the global seafloor calcite budget.

2. Study Area

The Ontong-Java Pleateau is historically an important site for studying the sedimentation and preservation of calcium carbonate (Berger & Killingley, 1982). It is characterized by a relatively slow sediment accumulation rate of less than 3 cm/kyr (Higgins et al., 1999) and a fairly strong latitudinal gradient in overlying water column production (Broecker et al., 1999; Kawahata et al., 2000). In order to limit the influence of latitude on the production and rain of carbonate, we picked four multicores collected on the R/V *Moana Wave Cruise 97-20* from a very limited latitude range (0.004–0.005°S; Table 1). The seawater bathing this plateau ranges from just undersaturated (Ω ~0.93) shallower than ~3,000 m water depth to more deeply undersaturated ($\Omega < 0.8$) deeper than ~3,800 m, as calculated using GLODAP v2.2019 data (Key et al., 2004; Olsen et al., 2016, 2019; Figure 1). The total sedimentation rate at this latitude is constrained at the upper end by sediment traps suspended at ~1,500 m that suggest an on-equator carbonate rain rate of 2.45 $g{\cdot}cm^{-2}{\cdot}kyr^{-1}$ (Kawahata et al., 2002). This rain has low organic matter content and a high percentage of calcium carbonate; the calcitic carbonate consists of about 45% coccoliths and 55% foraminifera (operationally defined by a 63 μm sieving cutoff of trap material; Kawahata et al., 1998, 2000).

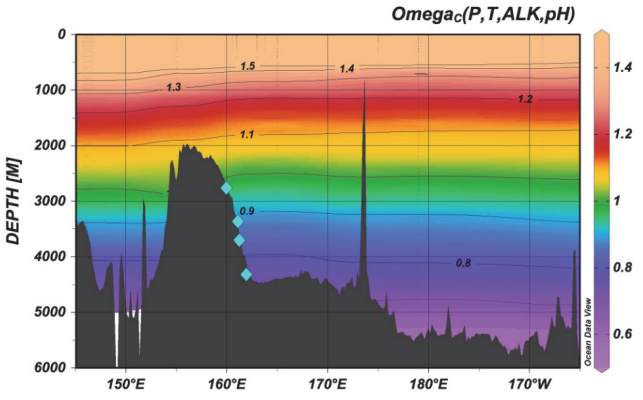

Figure 1. Ocean Data View longitudinal section of the Ontong-Java Plateau and bottom water chemistry, along with the depths of coring sites. Calcite saturation was calculated using the updated GLODAP v2.2019 database using the pH and Alkalinity pair (Olsen et al., 2016, 2019).

3. Methods

The upper 2 cm of the multicore tops were sectioned at 0.5-cm intervals, and stored in jars with buffered formalin solution (4% formalin in seawater, plus 10 g of "20 Mule Team Borax" per liter of solution), kept in the

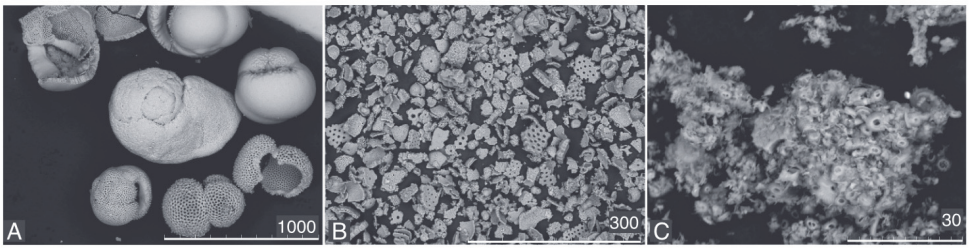

Figure 2. SEM images of sieved sediments from core MC55 at 2,767m. (a) >63 μm size fraction consisting of whole foraminiferal tests and large fragments. (b) 10–63-μm fraction consisting of foraminiferal fragments. (c) <10-μm fraction consisting of fine noncarbonate material and coccoliths. Lengths of scale bars are listed in the bottom-right corner of each plate.

Woods Hole Oceanographic Institution (WHOI) core repository. To separate coccoliths and foraminifera, we utilized the sieving method of Chiu and Broecker (2008) and Broecker and Clark (2009), with one modification. We used a 10 μm sieve instead of a 20-μm sieve to better capture the minimum in particle size frequency at 8 μm found by Frenz et al. (2005), which marks the boundary between coccolith and foraminifera fragment calcite. Inspection via scanning electron microscopy (SEM) confirmed that a 10-μm sieve more effectively removed small foraminiferal fragments from the smallest size fraction, compared to a 20-μm sieve (Figure S1 in the supporting information).

About 0.3–0.5 g of bulk sediment was sieved using tap water (Broecker & Clark, 2009) into three size fractions: >63, 10–63, and <10 μm. Vigorous sonication between sieving steps ensured that as much disaggregated clay and coccolith material was removed from the surfaces of larger particles as possible. Sonication continued until the largest particles, which settled to the bottom of the beaker, appeared pure white. Every sample was inspected via SEM to confirm separation between coccoliths and foraminifera and fragments. In the rest of the manuscript, we refer to the <10-μm fraction as either the fine fraction or coccolith fraction; the 10–63-μm fraction as fragments; and the >63-μm fraction as whole foraminifera. Total foraminifera are considered to be the sum of all calcite >10 μm.

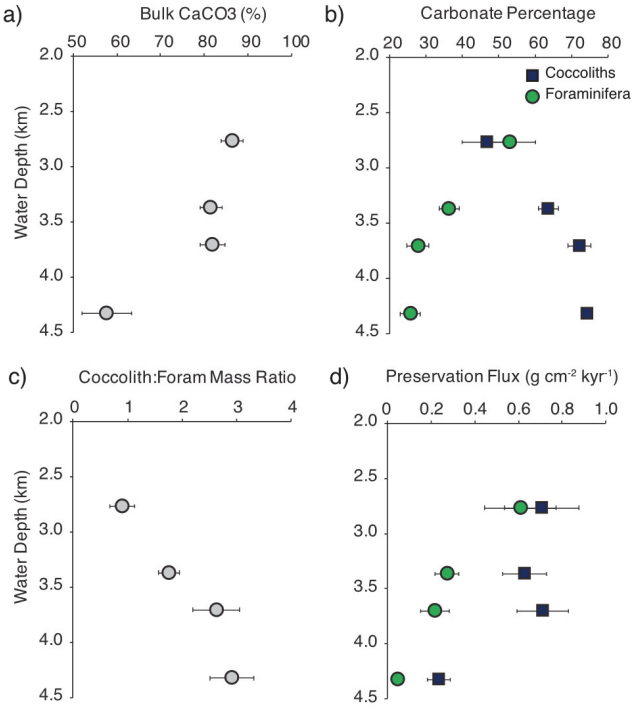

Figure 3. Upper 2-cm bulk carbonate and size fraction analysis. Data points and error bars are the mean and standard deviation, respectively, of all four 0.5-cm sections from the top 2-cm form each site. (a) Bulk percent carbonate in the upper 2 cm of the core top. (b) Coccolith (squares) and foraminifera (circles; whole plus fragment) contributions to the total carbonate. (c) Data in (b), plotted as the ratio of coccolith to foraminiferal carbonate. (d) calculated preservation fluxes using $R_{nc} = 0.2$ g·cm^{-2}·kyr^{-1}, with errors propagated from the mass data. Note the continuous decrease in foraminiferal preservation and the step change in coccolith preservation at 4,325 m.

The topmost (0–0.5 cm) and bottommost (1.5–2 cm) fractions of each core were analyzed for their radiocarbon content via high-precision AMS dating at the National Ocean Sciences Accelerator Mass Spectrometry Facility, using the small sample processing line. Between 2 and 8 mg of sieved sediment were used for $\Delta^{14}C$ analysis, with a split of the hydrolyzed CO_2 taken for $\delta^{13}C$ analysis.

We also conducted a leach test to determine if there was any secondary precipitation on the fine fraction. Two aliquots of the fine fraction carbonate from core MC55 (0–0.5 cm) were weighed into 0.5 ml combusted glass vials to which dilute HCl was added. The amount of HCl added was calculated to titrate 10% and 25% of the carbonate mass of the sample, respectively. Vials were mixed via pipette every 10–15 min until the pH of the solution was ~7. Solids were then left to settle and the neutralized acid was removed via pipette. The vials were then placed inside hydrolysis vessels and dried under vacuum. The resulting dry sediment was processed as a typical $CaCO_3$ radiocarbon sample.

Percent $CaCO_3$ and $\delta^{13}C$ were measured on a separate aliquot using a modified Picarro CRDS-Liaison system (Dong et al., 2019; Subhas et al., 2015). Between 0.8 and 3 mg of sediment sample was weighed into 12 ml Labco Exetainer vials with screw-top septum caps. Vials were then evacuated and manually acidified with 3 ml of 10% phosphoric acid. CO_2 was quantitatively stripped and analyzed on the Picarro-Liaison-Automate

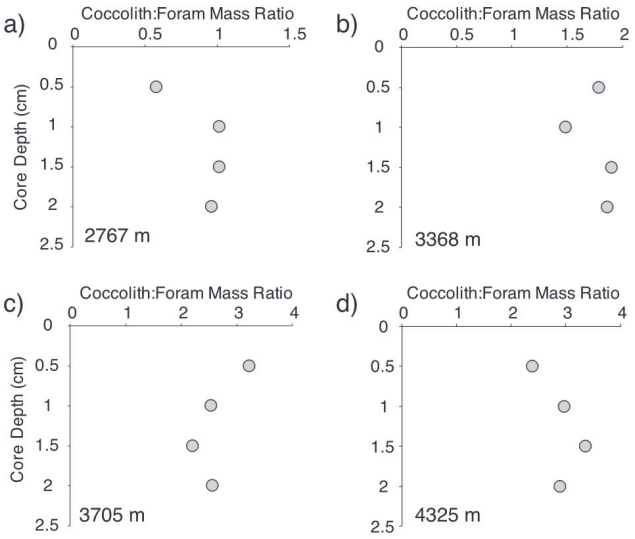

Figure 4. Downcore depth profiles of coccolith:foraminifera mass ratios. Subpanels a-d display data from the four cores, in order of water depth. Water depth of each site is shown in the bottom left-hand corner. Note the difference in *x* axis scales. Analytical weighing errors are smaller than the size of the points.

system. Total CO_2 was calibrated using a standard curve of pure Iceland Spar calcite. Carbon isotopic composition was calibrated using several isotopic standards and the isotopic composition of the internal standard, run over multiple analytical sessions (Iceland Spar; 1.5 ‰; Figure S2). All isotopic values were corrected using the transfer function displayed in Figure S2.

SEM images were collected on either a Hitachi TM3000 or a JEOL 840, both with Energy Dispersive X-ray Spectroscopy capability. For both instruments, samples were mounted on double-sided carbon tape (Ted Pella). The Hitachi TM3000 is an environmental SEM and required no further sample preparation. Samples imaged using the JEOL 840 were mounted and subsequently sputter-coated with 20 nm of graphite.

Trace metal analyses followed the procedure of Rongstad et al. (2017) in order to limit the influence of dissolution during cleaning on measured element ratios. Clay removal involving several steps of sonication using ultrapure (18.2 MΩ) water and methanol, and an oxidative cleaning step using NaOH-buffered hydrogen peroxide, was performed on all sediment size fractions. Measurements were conducted on a Thermo iCAP-Qc inductively coupled plasma mass spectrometer, intensity-matched to an in-house standard. ICP-MS data are provided in the supporting information. Aliquots of the surface coral JCp-1 demonstrate a long-term precision of 2.5% 2σ relative standard deviation.

4. Results

Each 0.5-cm interval was sieved into three fractions: >63, 10–63, <10 μm (Figure 2). The >63-μm fraction contains whole foraminifera and large fragments. The 10–63-μm fraction contains only foraminiferal fragments; some samples also contained radiolarians and diatoms. The <10-μm fraction contained carbonate and also noncarbonate particles. Sometimes, small foraminifera fragments were found; however, the majority of carbonate in this fraction, assessed by eye, was coccoliths.

All mass and isotopic data are provided as downloadable tables. In the manuscript, we present the data below in two general formats. Water column core top profiles are shown as the mean (data point) and standard deviation (error bar) of all four 0.5-cm sections, plotted against water depth. Downcore profiles within the top 2 cm are plotted as a function of depth in the core (cm), with separate plots for each core site.

Bulk coretop %$CaCO_3$ decreases as a function of water depth (Figure 3). The percentage of foraminifera also decreases, and by 3.7-km water depth, about 75% of the carbonate content is found in the fine fraction. These $CaCO_3$ percentages can be translated into preservation fluxes. At steady state, the fraction of total calcium

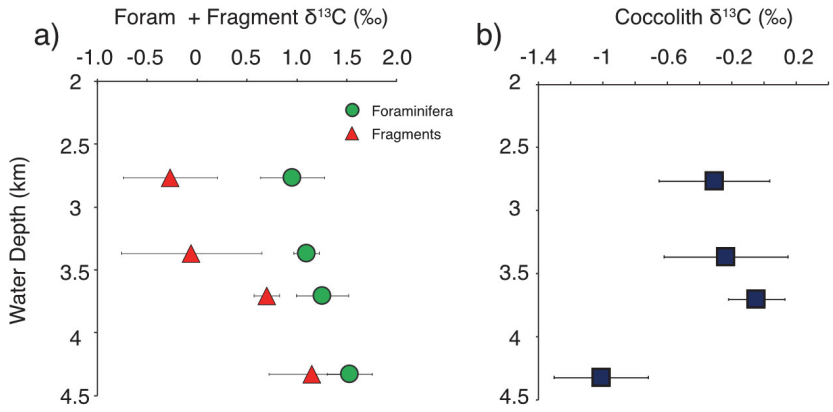

Figure 5. The mean carbon isotopic composition of size-fractionated core top carbonate samples. Error bars represent the standard deviation of all four 0.5-cm coretop sections. (a) $\delta^{13}C$ of the foraminiferal and fragment fractions. (b) $\delta^{13}C$ of the coccolith fraction.

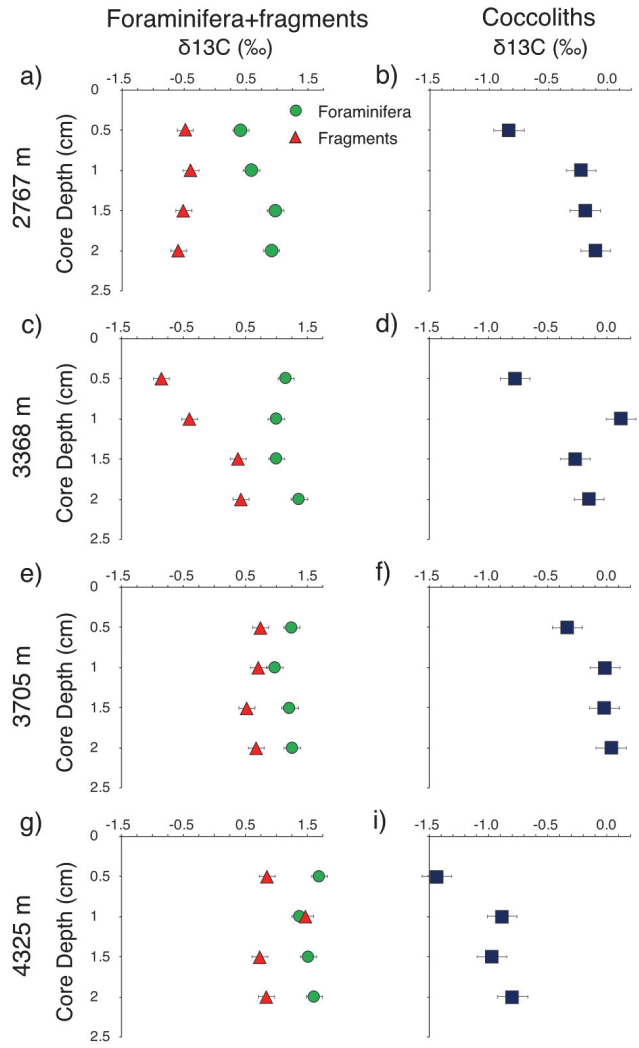

Figure 6. The carbon isotopic composition of size-fractions in each core top. Foraminifera and fragments are combined on the same axis (subpanels a,c,e,g)to show how the entire foraminiferal assemblage changes with depth. Coccolith data are displayed separately (subpanels b,d,f,i). Rows designate water depth. Error bars represent the standard deviation of the Picarro carbonate standard (0.13‰, $n = 8$).

carbonate in the bulk sediment mixed layer can be defined as

$$f_{\mathrm{CaCO_3}} = \frac{P_f + P_{co}}{P_f + P_{co} + R_{nc}}, \tag{1}$$

where $P = R - D$ is the preservation flux of coccoliths (co) or foraminifera (f) out of the sediment mixed layer. It is defined as the difference between the rain of carbonate material (R) and the total dissolution flux (D). R_{nc} is the rain of noncarbonate material. We define the fraction of foraminifera (f_f) in the carbonate as

$$f_f = \frac{P_f}{P_f + P_{co}}. \tag{2}$$

Rearranging this equation for the preservation of coccoliths gives

$$P_{co} = P_f \frac{1 - f_f}{f_f}. \tag{3}$$

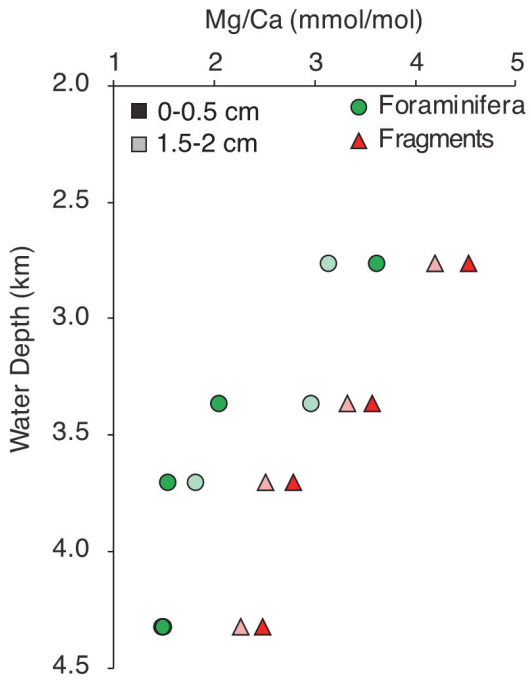

Figure 7. Mg/Ca of the whole foram (green circles) and fragment fractions (red triangles), measured on the 0–0.5 (solid) and 1.5–2 cm (translucent) sections. Both size fractions show a decrease in Mg/Ca with core depth.

Substituting this into equation (1), and rearranging for P_f, gives

$$P_f = f_f \cdot R_{nc} \cdot \frac{f_{CaCO_3}}{1 - f_{CaCO_3}}. \quad (4)$$

With a known value of R_{nc} at the Ontong-Java Plateau of 0.2 g·cm^{-2}·kyr^{-1} (Oxburgh, 1998) and measured values of f_f and f_{CaCO_3}, equations (3) and (4) can be used to calculate the steady-state preservation flux of coccoliths and foraminifera (Figure 3d).

Foraminiferal preservation flux decreases by over a factor of 6 with increasing water depth, from 0.6 g·cm^{-2} kyr^{-1}, to less than 0.1 g·cm^{-2}·kyr^{-1}. Coccolith preservation fluxes remain relatively constant at 0.7 g·cm^{-2}·kyr^{-1} before decreasing by about a factor of 3 at 4,325 m.

In the interval from 3,705 to 4,325 m, the simultaneous decrease in coccolith and foraminiferal preservation leads to an only modest increase in the coccoltih:foram mass ratio (Figures 3c and 3d). This decrease in preservation is concomitant with a significant drop in the bulk %$CaCO_3$ (Figure 3a).

Downcore profiles of coccolith to foraminiferal carbonate mass ratios show no consistent patterns within the top 2 cm at each site (Figure 4). However, in the shallowest core (2,767 m), the 0–0.5 cm mass ratio of 0.55 is about a factor of 2 smaller than the downcore mass ratios (0.5–2 cm), an observation that we return to below.

Profiles of core top foraminiferal and fragment δ^{13}C show an increase with water depth (Figure 5). The absolute value of foraminifera fragment δ^{13}C is also low relative to the whole foraminifera (Figure 5a). In contrast, coccolith calcite displays a different trend with water depth (Figure 5b), showing a similar pattern to coccolith preservation fluxes. Unlike foraminiferal calcite δ^{13}C, which becomes enriched with depth, coccolith calcite in the deepest core is slightly more negative than in shallower cores.

The downcore δ^{13}C data show some trends with core depth (Figure 6). In particular, the foraminiferal fraction δ^{13}C in the shallowest (2,767 m) core increases in the upper 1 cm of the sediment column. Deeper cores display relatively constant foraminiferal δ^{13}C downcore. The foraminifera fragment δ^{13}C profile at 3,368m shows an increase with depth in the core, and otherwise there is no trend in foraminifera fragment δ^{13}C downcore. Unlike foraminifera, all coccolith δ^{13}C profiles show an increase with depth. Coccolith δ^{13}C increases by about 0.4 to 0.8 permil, especially between 0–1 cm (Figure 6, right column).

The Mg/Ca of our bulk sieving fractions is shown in Figure 7 (All metal-calcium data are provided as downloadable material). We emphasize that these measurements are related to, but distinct from, Mg/Ca

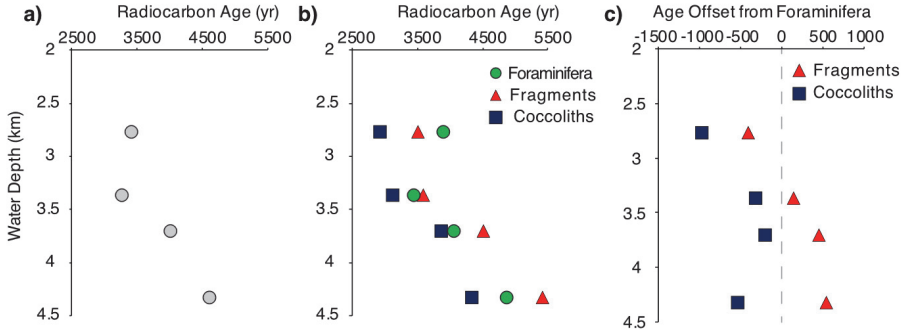

Figure 8. The water column profile of radiocarbon age for (a) bulk $CaCO_3$ and (b) size fractions. For clarity, we plot the mean values of the 0–0.5 and 1.5–2-cm sections from each site. For depth profiles, see Figure S3 in the supporting information. Panel (c) shows the radiocarbon age offsets of the fragment and coccolith fraction relative to whole foraminifera. Analytical AMS errors were on the order of 10–50 years and are smaller than the size of the points.

measurements of individual foraminifera picked from sediment cores. Whole foraminifera decrease in Mg/Ca from 3.4 to 1.5 mmol/mol. Similar to the pattern of $\delta^{13}C$ (Figure 5), foraminiferal fragment Mg/Ca is enriched relative to the whole foraminifera and shows a decrease from 4.4 to 2.4 mmol/mol. The Mg/Ca of fragments from 1.5–2 cm are consistently depleted relative to those from 0–0.5 cm. There is no clear trend in whole foram Mg/Ca from 0–0.5 cm to 1.5–2 cm.

Water column profiles of radiocarbon age (Figure 8) demonstrate an increase in bulk age with water depth. We observe age offsets between foraminifera, fragments, and coccoliths, of up to 1,000 years. Foraminifera fragments are younger than whole foraminifera at 2,767m, and transition to being older than whole foraminifera in the deeper cores. Coccolith fragments are consistently younger than whole foraminifera. There is no obvious trend in the coccolith-foraminifera age offset with water depth (Figure 8c).

Age offsets persist deeper into the core and are relatively consistent in the upper 2 cm (Figure S3). All cores show increasing radiocarbon age with core depth, with the exception of the bulk age in MC55 at 2,767 m, which stays constant. The strongest downcore age increase is evident in MC28 at 4,325 m.

5. Discussion

Dissolution at or above the sediment-water interface has long been shown to produce a trend of older bulk carbonate age with water depth (Broecker et al., 1991). We see this same trend in bulk radiocarbon age (Figure 8a), consistent with the previous studies on the Ontong-Java Plateau (Broecker et al., 1991, 1999), and with a body of literature arguing that a substantial portion of carbonate dissolution must occur at the sediment-water interface (Broecker et al., 1999; Hales & Emerson, 1996; Martin et al., 2000; Oxburgh, 1998; Oxburgh & Broecker, 1993).

The increase in coretop coccolith:foraminifera mass ratio with water depth (Figure 3) argues that this interface dissolution is primarily driven by the loss of foraminifera. This hypothesis is further supported by our downcore mass (Figure 4), $\delta^{13}C$ (Figure 6) and Mg/Ca data (Figure 7), which show strong trends with water depth, but no clear trends with core depth in the top 2 cm. Without detailed deep sediment trap data, we cannot differentiate between foraminiferal dissolution at the sediment-water interface and dissolution in the water column.

5.1. Why Do Foraminifera Dissolve Faster Than Coccoliths?

Our results suggest that foraminiferal calcite is different from coccolith calcite and that controls on its preservation are different from the controls on coccolith preservation. Indeed, Subhas et al. (2018) and Honjo and Erez (1978) showed that the dissolution rate of foraminifera, both per unit mass and per unit surface area, is faster than the dissolution rate of coccoliths. Hypotheses for this difference in dissolution rate have included coccolith surface features limiting dissolution (e.g., the density of defects or the presence of organic molecules; Honjo & Erez, 1978; Subhas et al., 2018), to their small size limiting their exposure to bottom water chemistry during sedimentation (Honjo & Erez, 1978). However, Subhas et al. (2018) showed that, near equilibrium, coccolith and inorganic calcite dissolve at a similar rate. Therefore, it may be more instructive to ask, "Why do foraminifera dissolve so quickly?"

Previous studies have suggested that foraminferal calcite is heterogeneous and that this heterogeneity leads to a spectrum of reactivity in seawater (Brown & Elderfield, 1996; Johnstone et al., 2011; Lohmann, 2010). Our results bear these species-specific results out at the assemblage scale: Dissolution-prone, ^{13}C-depleted and Mg-rich foraminifera or foraminiferal components appear to dissolve preferentially (Figures 5 and 7), leaving behind a relatively high $\delta^{13}C$ (low-Mg) whole foraminiferal component. The relative depletion in fragment ^{13}C compared to whole tests (Figures 5 and 6) supports this hypothesis, since test fragments must be derived from originally intact tests. Similarly, high-Mg fragments are most likely remnant pieces of high-Mg (and dissolution-prone) whole tests.

The dissolution of a low-$\delta^{13}C$, high-Mg, component of foraminiferal calcite has several possible explanations. First, pregametogenic calcite is enriched in Mg (Brown and Elderfield, 1996) and depleted in ^{13}C (Lohmann, 2010). Inner, pregametogenic calcite layers appear to dissolve preferentially, as documented by μ-computed tomography (CT) scanning (Johnstone et al., 2010), leaving behind Mg-depleted, partially dissolved tests (Johnstone et al., 2011). Second, small foraminifera typically have lower $\delta^{13}C$ than larger foraminifera of the same species (Berger et al., 1978; Elderfield et al., 2002). We confirmed visually that the shallowest core at 2,767 m contains the most small foraminifera (Figure S4) and that these small foraminifera

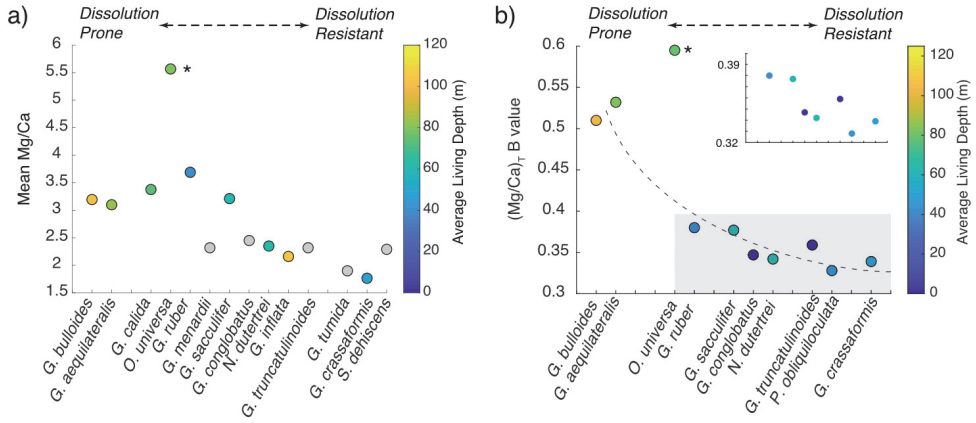

Figure 9. (a) Mean Mg/Ca from Elderfield et al. (2002) versus the dissolution index ranking of Thunell and Honjo (1981) for several species of planktic foraminifera. Color scale represents the mean living depth of each species, taken from Rebotim et al. (2017). Gray fill indicates no available living depth data. The Mg/Ca of *Orbulina universa*, marked by the asterisk, is anomalously high, an observation that has been made before (e.g., (Anand et al., 2003)). (b) A plot of the "*B*" value from the equation $(Mg/Ca)_T = B\exp(A \cdot T)$, as defined by Anand et al. (2003), against foraminiferal dissolution index. *B* data are taken from Table 3 assuming a fixed temperature sensitivity ($A = 0.09$). The inset is a zoom-in of the grayed region. The dashed line highlights the trend and is not a fit to the data. The *x* axes in the two plots are different because of the available mean Mg/Ca data (in panel a) and temperature-calibrated Mg/Ca data (in panel b).

are largely absent from every other core section. Finally, a dissolution-driven change in foraminiferal assemblage may contribute to our $\delta^{13}C$ and Mg/Ca trends (Le & Thunell, 1996).

The loss of magnesium as a function of dissolution in individual foraminiferal species has been known for decades (Anand et al., 2003; Brown & Elderfield, 1996; Elderfield et al., 2002; Johnstone et al., 2011; Klinkhammer et al., 2004). What distinguishes our measurements is the correlation between dissolution of the entire foraminiferal assemblage and its Mg/Ca content. This effect emerges above and beyond any intratest variability in Mg/Ca ratio.

A larger-scale relationship between foraminiferal Mg content and dissolution susceptibility is illustrated by plotting dissolution index data from Thunell and Honjo (1981) against the Metal-calcium ratio data from Elderfield et al. (2002) and Anand et al. (2003) (Figure 9a). Such a relationship was proposed specifically for *Globorotalia tumida* by Brown and Elderfield (1996), but not investigated systematically for all planktic species. Mg/Ca, measured on whole, well-preserved foraminifera from a core top in the North Atlantic, is negatively correlated to the dissolution index of Thunell and Honjo (1981) (Figure 9a).

For any given species, its Mg/Ca is set by temperature, and by a species-specific Mg incorporation factor (Anand et al., 2003): $(Mg/Ca)_T = B\exp(A \cdot T)$, where *A* is the Mg/Ca sensitivity to temperature in °C, and *B* is a species-specific, temperature-independent Mg-incorporation factor. Assuming a constant value for temperature sensitivity *A* across all species (Anand et al., 2003), the *B* value also scales with dissolution susceptibility (Figure 9b). Because this *B* value is independent of Mg-temperature effects, its variation between these species is recording temperature-independent aspects of Mg incorporation during biomineralization.

A large shift in foraminiferal assemblage associated with dissolution is observed on the Ontong-Java Plateau (Le & Thunell, 1996). Shallower than 2,500 m, assemblages are dominated by *Globigerinoides ruber* and *Globigerinita glutinata* (relatively Mg-rich and dissolution prone; Figure 9) and transition to > 80% *Pulleniatina obliquiloculata* (relatively Mg-poor and dissolution resistant Figure 9b) in deeper water. We therefore propose that the changes in Mg/Ca we observe at the assemblage scale are due to a combination of the preferential loss of Mg-rich test components, in addition to a species preservation effect, where high-Mg species are dissolved and low-Mg species are preserved.

These observations are at odds with inorganic calcite data, in which calcites with less than ~4 mol% Mg demonstrate the same solubility as Mg-free calcite (Bischoff et al., 1987; Mucci & Morse, 1984). Planktic foraminifera, which demonstrate low Mg contents of 1–4 mmol/mol Mg (Elderfield et al., 2002), should therefore not show any relationship between dissolution susceptibility and Mg content. Indeed,

solubility experiments showed no statistical difference between foraminiferal and inorganic calcite *Ksp′* (Morse et al., 1980).

At the same time, changes in Mg content as a function of dissolution are observed, above and below the calcite saturation horizon (Johnstone et al., 2011; Brown & Elderfield, 1996). Brown and Elderfield (1996) argued that even small Mg contents (5–16 mmol/mol) should increase calcite solubility, and therefore should shoal the saturation horizon for components of foraminiferal calcite that are enriched in Mg. We have demonstrated here a decrease in Mg/Ca at the assemblage level (Figure 7) and a strong, negative correlation between dissolution resistance and Mg/Ca content (Figure 9). These observations are bolstered by laboratory experiments that show preferential dissolution of a high Mg phase in both planktic (Klinkhammer et al., 2004) and benthic (Subhas et al., 2018) species.

To illustrate the relationship between Mg content (even at the subpercent level) and biogenic calcite reactivity, we calculate the sensitivity of assemblage-scale Mg/Ca to carbonate ion concentration. In units of mmol per μmol kg^{-1}, $\Delta Mg/Ca/\Delta CO_3^{2-} = 0.086$ for whole forams, 0.090 for fragments, and 0.064 for the whole assemblage (forams + fragments; see supporting information and Figure S5). These sensitivities are at the upper end of the Mg/Ca sensitivities calculated by Johnstone et al. (2011) for several planktic species (0.037–0.102), and a factor of 2–3 larger than the sensitivity of *G. tumida* to ΔCO_3^{2-} calculated from the data of Brown and Elderfield (1996) (0.033; supporting information). Our sensivitity is closest to that of *G. ruber* (0.102, Johnstone et al., 2011), a species that shows a large decrease in abundance from 2,500 to 4,000 m on the Ontong-Java Plateau (Le & Thunell, 1996). The broad agreement between species-specific Mg losses and our data suggests that a similar mechanism is occurring at the individual species and total assemblage scales and that the reactivity of foraminiferal calcite in general is related to its Mg content.

Why Mg-rich calcite is so susceptible to dissolution is still an open question. Although foraminiferal Mg/Ca content does not scale with habitation depth (Figure 9, Rebotim et al., 2017), Mg content does appear to scale with calcification depth (Anand et al., 2003; Bender et al., 1975) and therefore could be related to calcification rate (Lammers & Mitnick, 2019). However, authigenic calcites precipitated in equilibrium with seawater appear to contain more Mg than foraminiferal tests (Branson et al., 2015; Lammers & Mitnick, 2019), and it is therefore unlikely that Mg incorporation alone leads to less stable calcite. Alternatively, concentration of minor and trace elements has been linked to the primary organic membrane and the formation of amorphous calcium carbonate (Branson et al., 2016; de Nooijer et al., 2014; Politi et al., 2010; Wang et al., 2009). Amorphous calcium carbonate is highly soluble and unstable. Thus, susceptibility to dissolution may be related to the species-specific ability to transform impurity-rich amorphous calcium carbonate or quasi-crystalline $CaCO_3$ into pure calcite (Blue et al., 2017; Jacob et al., 2017).

In comparison, coccolithophores precipitate relatively pure calcite (i.e., $CaCO_3$ with very low cation substitution; Stoll et al., 2001; Young & Henriksen, 2003). Dissolution kinetics studies suggest that the slow coccolith dissolution rate could be due to the lack of defects on the coccolith surface or potentially due to the interaction between organics and the lith surface (Subhas et al., 2018). The low reactivity of coccolith calcite could be further related to the high degree of control that coccolithophores exert over biomineralization, compared to foraminifera which use seawater directly in their calcifying medium (Erez, 2003). We suggest that these differences in coccolith and foraminiferal calcite mineralogy, which appear to be linked to cation incorporation and potentially biomineralization strategy, exert a strong influence on their relative preservation in sediments.

5.2. Radiocarbon Age Offsets and Their Relationship to Dissolution

The mass, stable isotope, and Mg/Ca measurements discussed above suggest that much of the dissolution of foraminifera occurs at the sediment-water interface. At steady state, the rate of carbonate supply and burial are balanced, such that $\Delta^{14}C$ traces the mean residence time of solid carbonate in the sediment mixed layer (Broecker et al., 1991). Dissolution at or above the sediment-water interface reduces the supply of carbonate to the sediment and therefore generates a trend of increasing core top age with increasing dissolution. (Broecker et al., 1999) Dissolution within the sediment column has been referred to as "homogenous" dissolution because of an assumption that all carbonate within the sediment mixed layer dissolves at the same rate (Broecker et al., 1991, 1999; Oxburgh & Broecker, 1993). Because we are interested in the potential for different biogenic calcite phases to impact sedimentary calcite preservation, we instead use "within-sediment" dissolution.

Because dissolution at or above the sediment-water interface only modifies the $CaCO_3$ rain to the sediment and does not modify the inventory of bioturbated sediment, it should not produce age offsets between carbonate fractions (Barker et al., 2007). It is therefore puzzling that we observe radiocarbon age offsets between coccoliths, foraminifera, and foraminiferal fragments (Figure 8). In addition, if foraminifera dissolve preferentially within the sediment mixed layer, they should appear younger than coccoliths. Instead, coccoliths are consistently younger than foraminifera and their fragments. These coccolith-foraminifera age offsets are similar to observations made by Barker et al. (2007), in which more "reactive" foraminiferal fragments appear older than whole foraminifera. We consider several explanations for these coccolith-foraminifera $CaCO_3$ age offsets:

1. *Bioturbation*. If foraminifera are bioturbated deeper than coccoliths, then the effective inventory of foraminifera would be larger in the sediment mixed layer. A smaller coccolith inventory, and roughly equal fluxes of coccoliths and foraminifera, would lead to a shorter coccolith residence time (younger radiocarbon age) in the mixed layer. The experiments of Wheatcroft (1992) demonstrated that smaller particles are mixed deeper more quickly than larger particles. However, these experiments also showed that small and large particles are mixed to the same depth. We therefore expect no effect of bioturbation depth on relative mixed layer residence times and radiocarbon ages.
2. *Exhumation*. If the dissolution flux of carbonate exceeds the rain of carbonate from above, burrowing organisms begin to exhume older sediments. However, assuming that older foraminifera should still dissolve faster than older coccoliths, this erosion should leave behind an even older coccolith residue. Therefore, this cannot be the reason for our observed age offsets.
3. *Secondary precipitation*. If there is secondary precipitation of porewater dissolved inorganic carbon onto coccolith calcite, it could appear younger than foraminiferal calcite. However, radiocarbon ages of leached coccolith fractions show the same age, within error, as the untreated fraction (Data Set S1). Because coccolith calcite contains virtually no Mg, and calcite precipitated in equilibrium with seawater Mg/Ca $\sim$ 5 contains some Mg (Lammers & Mitnick, 2019; Oomori et al., 1987), we attempted to identify secondary calcite by the presence of Mg on coccolith surfaces. Energy Dispersive X-ray Spectroscopy spot-checks of coccolith calcite using JEOL 840 SEM detected little to no magnesium on coccolith surfaces (Figure S6). The spots which demonstrated trace amounts of magnesium also showed an enrichment in silicon, indicating the influence of fine clays. Therefore, it is unlikely that secondary precipitation is significantly affecting the radiocarbon age offsets observed here.
4. *Sediment winnowing/focusing*. Downslope transport of coccoliths would increase the coccolith:foraminifera mass ratio. If young coccoliths are transported from shallower sediment, then this transport could potentially bias the coccolith fraction to younger ages. Higgins et al. (1999) suggested that excess Th trends in Ontong-Java Plateau sediments, sometimes used as a tracer of sediment focusing processes, are not due to sediment focusing downslope, but instead are likely related to enhanced water column Th scavenging. The extent of sediment focusing at our site is therefore unconstrained, but probably minor.

Given the arguments against each of these four explanations, we explore one additional possibility in detail: that age offsets are related to the preferential dissolution of coccoliths within the sediment. If the observed age offsets are caused by coccolith dissolution, they necessitate that (a) coccoliths dissolve faster than foraminifera; and (b) that this dissolution happens within the sediment mixed layer.

Area-specific dissolution rates of coccoliths and foraminifera (i.e., in units of mass per unit surface area per time) have generally been measured in well-mixed conditions, where particles are stirred or shaken in a large volume of seawater. In these experiments, measured rates reflect the inherent reaction rate between carbonate and seawater, with no influence of diffusion and boundary layer dynamics (Sjoberg & Rickard, 1983; Subhas et al., 2015; Naviaux et al., 2019). In these experiments, coccoliths appear to dissolve more slowly than foraminifera whether normalized by mass, or by surface area (Honjo & Erez, 1978; Keir, 1980; Subhas et al., 2018). Therefore, we can say with some certainty that the area-specific dissolution rate of coccolith calcite is slower than that of foraminiferal calcite. However, the conditions in sediments need not be the same as in the water column, and dissolution studies of packed sediment beds demonstrate an influence of boundary-layer diffusion, and pore-water diffusion, on the bulk dissolution rate (Boudreau, 2013; Sulpis et al., 2017). Therefore, the dissolution behavior of coccoliths and foraminifera may be different within the sediment compared to the water column or at the sediment-water interface.

In order for dissolution to cause coccoliths to be younger than coexisting foraminifera, coccoliths must dissolve faster than foraminifera per unit mass within the sediment. One mechanism for this change in dissolution behavior is a switch from reaction-rate limited dissolution (favoring foraminiferal dissolution), to diffusion-rate limited dissolution within pore spaces (favoring coccolith dissolution). All other conditions held equal, diffusion limitation should scale as a function of total carbonate surface area. Since coccoliths have a larger specific surface area compared to foraminifera by a factor of ~2.4 (Subhas et al., 2018), they could contribute a larger percentage of the $CaCO_3$ dissolution flux, relative to their mass, once the system is limited by diffusion of carbonate ion in porewater.

This "rate switch" hypothesis is also consistent with downcore coccolith $\delta^{13}C$ increases (Figure 6), which suggest a change in the coccolith dissolution behavior within the sediment mixed layer. Unlike foraminifera, there is little evidence that coccolith calcite is heterogeneous in composition, particularly for any given species. However, coccolithophores exhibit a large range in carbon isotope vital effects (e.g., Bolton & Stoll, 2014; McClelland et al., 2017). In general, large coccolithophores demonstrate negative $\delta^{13}C$ and smaller coccolithophores demonstrate higher $\delta^{13}C$ (Bolton et al., 2016). The observed downcore shifts could therefore be explained by the dissolution of the more heavily calcified species within the sediment column.

Coccolith $\delta^{13}C$ appears to decrease between 3,705 and 4,325 m, in tandem with a decrease in coccolith preservation flux (Figure 3). This trend is opposite to the increase in foraminiferal $\delta^{13}C$ with decreasing foraminiferal preservation flux (Figures 3 and 5) and is also opposite to the downcore trends in coccolith $\delta^{13}C$ (Figure 6). However, this trend does appear consistent with the coccolith dissolution index of (Berger, 1973). The heavily calcified, ^{13}C-depleted *Coccosphaera leptopora* is very dissolution-resistant, compared to the less calcified, ^{13}C-enriched *Emiliania huxleyi*. Based on this index, then, we should expect a shift to lower $\delta^{13}C$ with increasing dissolution, as more dissolution-prone species are preferentially lost from the sediment. Why coccolith $\delta^{13}C$ increases with core depth, though, is difficult to reconcile with Berger's coccolith dissolution index. It is possible that, similar to coccolith-foraminiferal differences in reactivity, *C. leptopora* has a higher specific surface area and contributes more to the within-sediment dissolution flux. We do not have a satisfactory explanation for these seemingly contradictory observations.

Nevertheless, the $\Delta^{14}C$ results argue for within-sediment dissolution of coccoliths. We constructed a simple model of carbonate rain and dissolution to estimate the magnitude of age offsets caused by this rate-switch hypothesis. The model scales with measured parameters, such as the rain of noncarbonate material (R_{nc}), and the relative ratios of coccolith and foraminiferal specific dissolution rates and surface areas. We start with the definition of radiocarbon age-based residence time t (Broecker et al., 1999):

$$t_{\text{carb}} = \tau log\left(1 + \frac{m_{\text{carb}}}{R_{s,\text{carb}} \cdot \tau}\right), \tag{5}$$

where $\tau = 1/8,267\ \text{year}^{-1}$ is the mean life of radiocarbon. The steady-state concentration of carbonate m_{carb} is defined in terms of the sediment density $\rho = 1\ \text{g/cm}^3$, the mixed layer thickness $h = 10$ cm, the total amount of carbonate and noncarbonate rain R_{carb} and R_{nc}, and the total amount of carbonate dissolution, D_{carb}:

$$m_{\text{carb}} = \rho \cdot h \cdot \frac{R_{\text{carb}} - D_{\text{carb}}}{R_{\text{carb}} - D_{\text{carb}} + R_{nc}}. \tag{6}$$

The total dissolution flux can be further divided into within-sediment (w) and interface (i) components, that is, $D_{\text{carb}} = D_w + D_i$. This leads to the definition of two new dissolution terms. First, $R_{s,\text{carb}} = R_{\text{carb}} - D_i$ is the total rain minus the dissolution flux at the sediment-water interface, and therefore represents the flux of carbonate incorporated into the sediment mixed layer. Second, we parameterize within-sediment dissolution by dissolving a fraction of $R_{s,\text{carb}}$: $D_w = f_w \cdot R_{s,\text{carb}}$. Coccoliths and foraminifera are then assigned specific rain rates (R_{carb}), interface dissolution terms (D_i), and within-sediment dissolution terms (D_w). The total carbonate rain values and partitioning of coccolith to foraminiferal rain are taken from sediment trap data (Kawahata et al., 2002): $R_{\text{carb}} = 2.45\ \text{g}\cdot\text{cm}^{-2}\cdot\text{kyr}^{-1}$, and is partitioned as 54% foraminifera and 46% coccoliths. We also assume that productivity has remained relatively constant over the last 5–10 kyr, such that our measurements reflect a true steady state between production and burial. Dissolution at or above the sediment-water interface (D_i) preferentially dissolves foraminifera by a factor of 2: $D_{i,f} = 2 \cdot D_{i,co}$, based on the factor of 2 faster dissolution rate normalized by mass found by (Subhas et al., 2018). Within-sediment

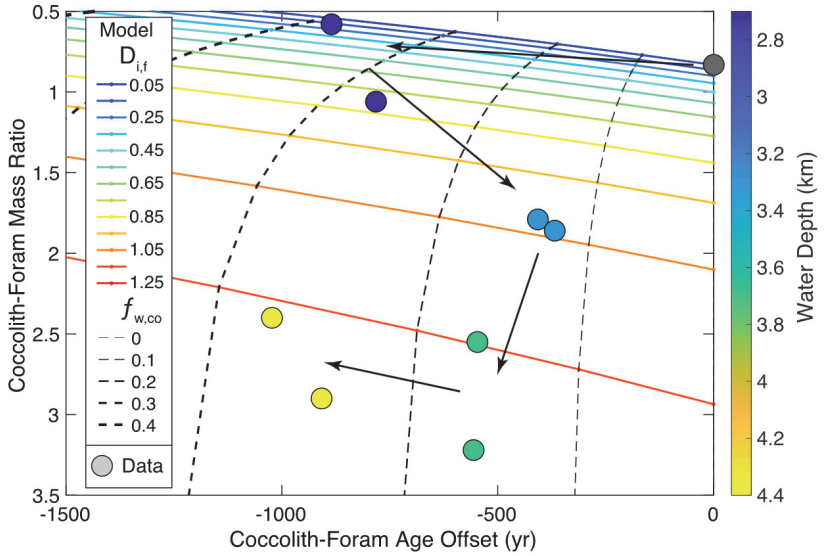

Figure 10. Model-data comparison plotting age offset and coccolith-foraminifera mass ratio for a simple model of interface and sediment dissolution. The dashed black vertical lines show different values of the fraction of the rain dissolved within the sediments ($f_{w,co}$), assuming that within-sediment coccolith dissolution is a factor of 2.4 faster than foraminiferal dissolution. The lines show $f_{w,co}$ values increasing from 0 to 0.4, moving from right to left. The solid, colored horizontal lines show the rate of interface dissolution ($D_{i,f}$, in g·cm^{-2} kyr^{-1}), assuming that interface dissolution for foraminifera is a factor of 2 faster than for coccoliths. The lines show foraminiferal dissolution rates increasing from 0.05 (top, blue line) to 1.25 (bottom, red line). Data (large circles, colored by water depth) are plotted on top of the model output, with the gray point being the composition of fresh carbonate rain (Kawahata et al., 2002). For each core the 0–0.5 and 1.5–2.0 cm data are plotted. This data-model comparison suggests more within-sediment dissolution in the shallowest core ($f_{w,co} \sim 0.3$), and an increasing influence of interface dissolution at greater water depth.

dissolution (D_w) is scaled to the coccolith/foraminifera surface area ratio (10.4/4.4 = 2.4 Subhas et al. (2018): $D_{w,f} = f_w \cdot R_{s,f}$ and $D_{w,co} = 2.4 \cdot f_w \cdot R_{s,co}$). In this way, analogous equations for the age of coccoliths (co) and foraminifera (f) can be derived. Substituting the two dissolution terms and the foraminiferal and coccolith scaling factors into equation (5), and rearranging, we diagnose age offsets between coccoliths and foraminifera:

$$t_f - t_{co} = \tau \log\left(1 + \frac{\rho \cdot h}{\tau} \frac{1 - f_w}{(1 - f_w)(R_f - 2 \cdot D_i) + R_{nc}}\right) - \tau \log\left(1 + \frac{\rho \cdot h}{\tau} \frac{1 - 2.4 \cdot f_w}{(1 - 2.4 \cdot f_w)(R_{co} - D_i) + R_{nc}}\right). \quad (7)$$

The two terms which can now vary are D_i and f_w. We construct a matrix of interface (D_i = 0.05–1.25 g·cm^{-2}·kyr^{-1}) and within-sediment dissolution fluxes (f_w = 0–0.4, i.e., 0–40% of the foraminiferal rain dissolved within the sediment), and then calculate the age offsets associated with these within-sediment/interface dissolution pairs using equation (7). Because this model inherently calculates the steady-state preservation of coccoliths and foraminifera, this modeled preservation ratio is also compared to the measured mass ratio in sediments.

Model calculations are compared to data in Figure 10. The radiocarbon age of foraminifera was treated as the mass-weighted mean of the >63 and 10–63 μm fraction radiocarbon ages. The carbonate rain composition from Kawahata et al. (2000, 2002) is shown by the gray point at the right-hand side of the plot. At the limit of only interface dissolution, we should observe an increase in the mass ratio of coccoliths to foraminifera, but no age offset (i.e., only vertical shifts in Figure 10). At the limit of only homogeneous/within-sediment dissolution, the mass ratio should decrease, and coccoliths should become younger than foraminifera (i.e., data should plot toward the top left of Figure 10).

Comparing our data to our model, deeper cores generally plot along a larger interface dissolution iso-line (larger D_i; quasi-horizontal lines in Figure 10). In other words, the amount of dissolution at or above the sediment water interface increases with depth. This observation is consistent with previous findings that much of the dissolution driving bulk sediment radiocarbon age occurs at the sediment-water interface (Broecker et al., 1991, 1999; Hales, 2003; Martin et al., 2000; Oxburgh & Broecker, 1993; Oxburgh, 1998). All of our mass, stable istotope, and radiocarbon data, combined with these model results, suggest that this interface dissolution is primarily driven by the selective dissolution of foraminifera.

Assuming that the carbonate rain is 54% foraminifera as constrained by sediment traps at 1,000 m (Kawahata et al., 2000, 1998), the low coccolith-foraminifera mass ratio of 0.5 at 2,767 m (Figure 4a) requires the preferential dissolution of coccoliths at this site. The surface area argument above suggests that preferential dissolution of coccoliths occurs within diffusively limited pore waters. This shallowest core therefore requires a larger dissolution flux within the sediment (farther to the left in Figure 10). In particular, the age offset of about 1,000 years between coccoliths and foraminifera imply that about 30% of the coccolith rain is dissolved within the sediment (vertically oriented, dashed lines in Figure 10). This hypothesis was raised, but dismissed based on a lack of evidence, by Broecker and Clark (2003) to reconcile their foraminiferal size/weight dissolution indices and porewater saturation data from the Ceara Rise (Martin and Sayles, 1996).

Such a large dissolution flux within the sediment is not surprising. Near the saturation horizon, much of the dissolution is driven by respiration of organic carbon within the sediment column (Hales & Emerson, 1996, 1997; Hales, 2003). In particular, a porewater pH profile at a 2,900 m deep site on the Ontong Java Plateau ($\Omega \sim 0.91$, similar to $\Omega \sim 0.93$ at our 2,767-m site, Table 1) shows a distinct pH minimum at 1 cm core depth (Hales & Emerson, 1996), indicating significant organic matter respiration within the sediment column (Emerson & Bender, 1981). These pH profiles, and previous radiocarbon age studies, estimate that about 30% of carbonate rain is dissolved in sites at or near the saturation horizon at sites on the Ontong-Java Plateau and the Ceara Rise (Broecker & Clark, 2003), consistent with our model results. The diffusively limited dissolution of coccolith calcite within the sediment column at 2,767 m may therefore be driven by production of respiratory CO_2, a signal which is manifested in both the downcore mass ratio of coccoliths to foraminifera, and in the radiocarbon age offset between these calcite forms.

We observe a sharp decrease in coccolith preservation at 4,325 m compared to 3,705 m (Figure 3). The large age offset observed at this site requires that this decrease in preservation is due to within-sediment coccolith dissolution, which appears to prevent the continuous increase in coccolith-foram mass ratio despite the low preservation of foraminifera. It is possible that the amount of within-sediment dissolution increases because bottom water undersaturation is larger-undersaturation may persist deeper in the sediment, allowing more dissolution to take place within the diffusively-limited sediments. It is also possible that coccoliths dissolve faster in this core, because of the nonlinear dependence of dissolution rate on degree of undersaturation (Dong et al., 2018; Subhas et al., 2018), which predicts a large increase in dissolution rate roughly where MC28 sits in the water column ($\Omega \sim 0.75$; Figure 1 and Table 1). This increased rate of coccolith dissolution, combined with the almost complete lack of foraminifera at this site, both contribute to the significant drop in total carbonate mass at 4,325 m, that is, the initiation of the calcite lysocline.

5.3. Implications for the Global $CaCO_3$ Budget

The preferential dissolution of foraminifera at or above the sediment-water interface means that the calcite content of many marine sediments may not reflect the production of foraminiferal calcite in overlying surface waters. Foraminiferal and coccolith calcite production is relatively hard to constrain; Erez (2003) estimates that open-ocean calcification is roughly equally split between coccolithophores and foraminifera. This estimate is consistent with the global compilation of coccolith:foraminifera mass ratios in sediments above the saturation horizon (Broecker & Clark, 2009). Tambutté et al. (2011), on the other hand, suggests that foraminifera produce about twice as much calcite as coccolithophores. Baumann et al. (2004) also showed that the coccoltih:foraminifera mass ratio is higher in the subpolar South Atlantic than in the Western Equatorial Atlantic, and suggested that this difference was due to changes in ecological regime.

Our study shows that carbonate sediments below the saturation horizon on the Ontong-Java Plateau are enriched in coccoliths relative to foraminifera. In fact, increases in fine-grained sediment below the saturation horizon have been observed previously in the Pacific (Broecker & Clark, 1999) and the Atlantic (Hales and Emerson, 1997) basins. These fine-grained carbonate sediments have since been recognized as coccolith-dominated (Broecker & Clark, 2009; Chiu & Broecker, 2008; Frenz et al., 2005).

Table 2
Global seafloor area percentage (from Menard & Smith, 1966) and the global binned median coretop calcium carbonate content from David Archer (Archer, 1996)

Seafloor bin (km)	SF area (%)	$CaCO_3$ (%)	Coccolith (%)	Seafloor area ($\times 10^{12}$ m^2)	Mass cocco ($\times 10^{16}$ g)	Mass foram ($\times 10^{16}$ g)	Ratio
0.2–1	4	3.0	45	1.7	0.2	0.3	0.8
1–2	4	46.0	45	0.6	3.6	4.4	0.8
2–3	9	49.0	50	1.2	8.2	8.2	1.0
3–4	21	54.8	65	2.7	29.6	15.9	1.9
4–5	32	22.8	75	4.6	21.6	7.2	3.0
5–6	21	0.8	75	3.2	0.5	1.7	3.0
6–7	1	0.2	75	0.1	0.007	0.002	3.0
TOTAL	—	—	—	141	64	36	1.8

Note. Seafloor bins are depth ranges in kilometers. We excluded the upper 200 m because of the large coastal areas that are dominated by terrigenous input and coral reef calcification. We also assume a coccolith:foram ratio depth distribution from the data presented in this paper (Figure 3), and a coccolith:foraminifera rain above the saturation horizon from Kawahata et al. (2002).

The preferential dissolution of foraminifera, and a shift toward coccolith-dominated carbonate sediments below the saturation horizon, should therefore exert significant global control on the type of calcite buried on the seafloor. Given modern ocean floor hypsometry, about 74% of the ocean's area is found between 3 and 6 km (Menard & Smith, 1966). The saturation horizon in the Atlantic ocean is found quite deep at around 4.5 km; in the Pacific it is on average at around 3 km (Key et al., 2004). In both basins, therefore, a large area of carbonate-rich sediment actually sits below the saturation horizon.

We provide below an estimate of the relative contribution of foraminifera and coccoliths to surface ocean sediments, assuming that foraminifera dissolve preferentially as observed on the Ontong-Java Plateau, and a delivery of coccoliths (45%) and foraminifera (55%) to surface sediments measured by sediment traps (Kawahata et al., 2002). Although there is a large range in the coccolith:foraminifera ratio in surface sediments (20–95%), the mean (median) value is 54 (53)% (Broecker & Clark, 2009). In the absence of more measurements of size-fractionated carbonate below the saturation horizon, we take this as a first-order estimate. We multiply each 1-km depth interval of seafloor area (Menard & Smith, 1966) by the global median carbonate composition of that depth interval (Archer, 1996), and assuming unit density (i.e., 1 g/cm^3), calculate the mass of carbonate found in the upper centimeter of sediment at that depth. This calculation shows that, globally, coccoliths outweigh foraminifera in surface sediments by a factor of 1.8 (Table 2).

Given the difference in preservation fluxes shown here, and the importance of calcite accumulation below the saturation horizon, changes in the ratio of foraminiferal to coccolithophore calcification may influence the shape of the lysocline through geologic time. Si and Rosenthal (2019) recently proposed that a decrease in coccolithophore calcification may have caused a decoupling between carbonate accumulation and saturation state over the Neogene. Coccolith:foraminifera production ratios also may have varied over glacial-interglacial cycles, which in turn may have influenced the large changes in lysocline shape and thickness over the Pleistocene (Farrell & Prell, 1989). In this way, the mineralogies of coccolith and foraminiferal calcite may provide distinct feedbacks to the global climate system through both biological and chemical compensation mechanisms (Boudreau et al., 2018). And since coccoliths tend to have lower $\delta^{13}C$ values than planktic foraminifera, shifts in the coccolith:foraminifera burial ratio could influence the $\delta^{13}C$ of dissolved inorganic carbon. Investigation of how these ratios changed through the Pleistocene would contribute to our understanding of the linkage between glacial-interglacial productivity changes, carbonate compensation, ocean saturation state, and atmospheric pCO_2 (Sigman & Boyle, 2000).

6. Conclusion

We have demonstrated distinct preservation patterns of coccolith and foraminiferal calcite as a function of water depth on the Ontong-Java Plateau. Foraminifera appear to dissolve continuously as a function of water depth, whereas coccoliths show an abrupt decrease in preservation at 4,325 m, well below the calcite saturation horizon. Accompanying this trend in foraminiferal preservation are an increase in foraminiferal

$\delta^{13}C$, a decrease in Mg/Ca, and an increase in bulk $\Delta^{14}C$ age. These observations, together with the lack of trends in these isotopic and elemental values within the top 2 cm of the sediments, suggest that foraminiferal dissolution takes place at the sediment-water interface, not within sediments. The sensitivity of the entire foraminiferal assemblage Mg/Ca to water column saturation state ($\Delta Mg/Ca \sim 0.064\Delta CO_3^{2-}$) is similar to that measured for multiple individual species' Mg/Ca sensitivities, suggesting that a similar Mg-dissolution mechanism is setting the assemblage-scale preservation of foraminiferal calcite. Given the change in foraminiferal assemblage with depth, our observed Mg/Ca trends, and the strong negative relationship between a foraminiferal species' Mg incorporation factor and its dissolution susceptibility, we suggest that differences in foraminiferal biomineralization are likely driving the spectrum of reactivity observed between foraminifera.

In contrast to foraminiferal dissolution at the sediment-water interface, these data suggest that coccoliths dissolve faster within sediments, where diffusion limitation makes dissolution rate sensitive to the higher specific surface area of coccoliths compared to foraminifera. Despite a large dissolution flux of foraminifera, coccoliths appear younger than foraminifera by ~1,000 radiocarbon years at the shallowest site near the calcite saturation horizon ($\Omega \sim 0.93$). A model of coccolith and foraminiferal calcite rain rates, relative dissolution rates, and specific surface areas, implies that about 30% of the coccolith rain is dissolved within the sediment column. Age offsets persist at deeper sites and are the largest at 4,325 m, where the preservation of coccoliths sharply decreases. This site sits at a water column $\Omega \sim 0.75$, at approximately the value where laboratory studies predict a sharp increase in dissolution rate of coccolith calcite (Subhas et al., 2018).

Finally, our preservation trends suggest that coccoliths outweigh foraminifera in the global seafloor $CaCO_3$ inventory by a factor of 1.8.

Acknowledgments
A. V. S. thanks the NOSAMS facility and the WHOI/NOSAMS postdoc scholar program, James Funds, and the Bessette family for funding and support. A. Q. acknowledges Williams College research and travel funds. We thank the Stanley W. Watson Director's Discretionary Fund for the Picarro-Automate analyzer. We thank Ellen Roosen at the WHOI core repository for help with sample identification and sectioning. Thanks to Gretchen Swarr and the WHOI plasma mass spectrometry facility. Finally, we thank Bill Martin and Wally Broecker for enlightening discussions on dissolution and radiocarbon dating of deep ocean sediments. All data are included as supporting information files and are archived with NOAA's World Data Service for Paleoceanography (WDS Paleo; https://www.ncdc.noaa.gov/paleo/study/28150).

References

Adelseck, C. G. (1977). Dissolution of deep-sea carbonate: Preliminary calibration of preservational and morphologic aspects. *Deep Sea Research*, *24*(12), 1167–1185.

Anand, P., Elderfield, H., & Conte, M. H. (2003). Calibration of Mg/Ca thermometry in planktonic foraminifera from a sediment trap time series. *Paleoceanography*, *18*(2), 1050. https://doi.org/10.1029/2002PA000846

Archer, D., Kheshgi, H., & Maier-Reimer, E. (1998). Dynamics of fossil fuel CO_2 neutralization by marine $CaCO_3$. *Global Biogeochemical Cycles*, *12*(2), 259–276.

Archer, D. E. (1996). An atlas of the distribution of calcium carbonate in sediments of the deep sea. *Global Biogeochemical Cycles*, *10*(1), 159–174. https://doi.org/10.1029/95GB03016

Barker, S., Broecker, W., Clark, E., & Hajdas, I. (2007). Radiocarbon age offsets of foraminifera resulting from differential dissolution and fragmentation within the sedimentary bioturbated zone. *Paleoceanography*, *22*, 337, PA2205. https://doi.org/10.1029/2006PA001354

Baumann, K.-H., Bockel, B., & Frenz, M. (2004). Coccolith contribution to south Atlantic carbonate sedimentation. In H. R. Thierstein, & J. R. Young (Eds.), *Coccolithophores: From molecular processes to global impact* (pp. 367–402). Berlin, Heidelberg: Springer Berlin Heidelberg. Retrieved from. https://doi.org/10.1007/978-3-662-06278-4_14

Bender, M. L., Lorens, R. B., & Williams, D. F. (1975). Sodium, magnesium and strontium in the tests of planktonic foraminifera. *Micropaleontology*, *21*(4), 448.

Berger, W. H. (1973). Deep-sea carbonates: Evidence for a coccolith lysocline. *Deep Sea Research and Oceanographic Abstracts*, *20*(10), 917–921.

Berger, W. H., Killingley, J., & Vincent, E. (1978). Stable isotopes in deep-sea carbonates-box core erdc-92, west equatorial Pacific. *Oceanologica Acta*, *1*(2), 203–216.

Berger, W. H., & Killingley, J. S. (1982). Box cores from the equatorial Pacific: ^{14}C sedimentation rates and benthic mixing. *Marine Geology*, *45*(1-2), 93–125.

Bischoff, W. D., Mackenzie, F. T., & Bishop, F. C. (1987). Stabilities of synthetic magnesian calcites in aqueous solution: Comparison with biogenic materials. *Geochimica et Cosmochimica Acta*, *51*(6), 1413–1423.

Blue, C. R., Giuffre, A., Mergelsberg, S., Han, N., De Yoreo, J. J., & Dove, P. M. (2017). Chemical and physical controls on the transformation of amorphous calcium carbonate into crystalline $CaCO_3$ polymorphs. *Geochimica et Cosmochimica Acta*, *196*(C), 179–196.

Bolton, C. T., Hernandez-Sanchez, M. T., Fuertes, M.-A., Gonzalez-Lemos, S., Abrevaya, L., Mendez-Vicente, A., et al. (2016). Decrease in coccolithophore calcification and CO_2 since the middle Miocene. *Nature Communications*, *7*(1), 1–13.

Bolton, C. T., & Stoll, H. M. (2014). Late Miocene threshold response of marine algae to carbon dioxide limitation. *Nature*, *500*(7464), 558–562.

Boudreau, B. P. (2013). Carbonate dissolution rates at the deep ocean floor. *Geophysical Research Letters*, *40*, 744–748. https://doi.org/10.1029/2012GL054231

Boudreau, B. P., Middelburg, J. J., & Luo, Y. (2018). The role of calcification in carbonate compensation. *Nature Geoscience*, 1–8.

Branson, O., Bonnin, E. A., Perea, D. E., Spero, H. J., Zhu, Z., Winters, M., et al. (2016). Nanometer-scale chemistry of a calcite biomineralization template: Implications for skeletal composition and nucleation. *Proceedings of the National Academy of Sciences*, *113*(46), 12934–12939.

Branson, O., Read, E., Redfern, S., Rau, C., & Elderfield, H. (2015). Revisiting diagenesis on the Ontong Java Plateau: Evidence for authigenic crust precipitation in *Globorotalia tumida*. *Paleoceanography*, *30*, 1490–1502. https://doi.org/10.1002/2014PA002759

Broecker, W., & Clark, E. (2009). Ratio of coccolith $CaCO_3$ to foraminifera $CaCO_3$ in late Holocene deep sea sediments. *Paleoceanography*, *24*, 1, PA3205–11. https://doi.org/10.1029/2009PA001731

Broecker, W. S., & Clark, E. (1999). $CaCO_3$ size distribution: A paleocarbonate ion proxy. *Paleoceanography*, *14*, 596–604. https://doi.org/10.1029/1999PA900016

Broecker, W. S., & Clark, E. (2003). Pseudo dissolution of marine calcite. *Earth and Planetary Science Letters*, *208*(3-4), 291–296.

Broecker, W. S., Clark, E., McCorkle, C. D., Hajdas, I., & Bonani, G. (1999). Core top C-14 ages as a function of latitude and water depth on the Ontong-Java plateau. *Paleoceanography*, *14*, 13–22.

Broecker, W. S., Klas, M., Clark, E., Bonani, G., Ivy, S., & Wolfli, W. (1991). The influence of CaCO3 dissolution on core top radiocarbon ages for deep-sea sediments. *Paleoceanography*, *6*, 593–608. https://doi.org/10.1029/91PA01768

Brown, S. J., & Elderfield, H. (1996). Variations in Mg/Ca and Sr/Ca ratios of planktonic foraminifera caused by postdepositional dissolution: Evidence of shallow Mg-dependent dissolution. *Paleoceanography*, *11*, 543–551. https://doi.org/10.1029/96PA01491

Chiu, T. C., & Broecker, W. S. (2008). Toward better paleocarbonate ion reconstructions: New insights regarding the $CaCO_3$ size index. *Paleoceanography*, *23*, PA2216. https://doi.org/10.1029/2008PA001599

de Nooijer, L. J., Spero, H. J., Erez, J., Bijma, J., & Reichart, G. J. (2014). Biomineralization in perforate foraminifera. *Earth Science Reviews*, *135*(C), 48–58.

Dong, S., Berelson, W. M., Rollins, N. E., Subhas, A. V., Naviaux, J. D., Celestian, A. J., et al. (2019). Aragonite dissolution kinetics and calcite/aragonite ratios in sinking and suspended particles in the North Pacific. *Earth and Planetary Science Letters*, *515*, 1–12.

Dong, S., Subhas, A. V., Rollins, N. E., Naviaux, J. D., Adkins, J. F., & Berelson, W. M. (2018). A kinetic pressure effect on calcite dissolution in seawater. *Geochimica et Cosmochimica Acta*, *238*, 411–423.

Elderfield, H., Vautravers, M., & Cooper, M. (2002). The relationship between shell size and Mg/Ca, Sr/Ca, £^{18}O, and £^{13}C of species of planktonic foraminifera. *Geochemistry, Geophysics, Geosystems*, *3*(8), 1–13. https://doi.org/10.1029/2001GC000194

Emerson, S., & Bender, M. (1981). Carbon fluxes at the sediment-water interface of the deep-sea: Calcium carbonate preservation. *Journal of Marine Research*, *39*, 139–162.

Erez, J. (2003). The source of ions for biomineralization in foraminifera and their implications for paleoceanographic proxies. *Reviews in Mineralogy and Geochemistry*, *54*(1), 115–149.

Farrell, J. W., & Prell, W. L. (1989). Climatic change and CaCO3 preservation: An 800,000 year bathymetric reconstruction from the central equatorial Pacific. *Paleoceanography*, *4*, 447–466. https://doi.org/10.1029/PA004i004p00447

Frenz, M., Baumann, K. H., Boeckel, B., Hoppner, R., & Henrich, R. (2005). Quantification of foraminifer and coccolith carbonate in South Atlantic surface sediments by means of carbonate grain-size distributions. *Journal of Sedimentary Research*, *75*(3), 464–475.

Hales, B. (2003). Respiration, dissolution, and the lysocline. *Paleoceanography*, *18*. https://doi.org/10.1029/PA004i004p00447

Hales, B., & Emerson, S. (1996). Calcite dissolution in sediments of the Ontong-Java Plateau: In situ measurements of pore water O_2 and pH. *Global Biogeochemical Cycles*, *10*(3), 527–541.

Hales, B., & Emerson, S. (1997). Calcite dissolution in sediments of the Ceara Rise: In situ measurements of porewater O_2, pH, and CO_2 (aq). *Geochimica et Cosmochimica Acta*, *61*(3), 501–514.

Higgins, S. M., Broecker, W., Anderson, R., McCorkle, D. C., & Timothy, D. (1999). Enhanced sedimentation along the equator in the western Pacific. *Geophysical Research Letters*, *26*(23), 3489–3492. https://doi.org/10.1029/1999GL008331

Honjo, S., & Erez, J. (1978). Dissolution rates of calcium carbonate in the deep ocean; an in-situ experiment in the North Atlantic Ocean. *Earth and Planetary Science Letters*, *40*, 287–300.

Jacob, D.E., Wirth, R., Agbaje, O.B.A., Branson, O., & Eggins, S. M. (2017). Planktic foraminifera form their shells via metastable carbonate phases. *Nat Commun*, *8*, 1265. https://doi.org/10.1038/s41467-017-00955-0

Johnstone, H. J. H., Schulz, M., Barker, S., & Elderfield, H. (2010). Inside story: An X-ray computed tomography method for assessing dissolution in the tests of planktonic foraminifera. *Marine Micropaleontology*, *77*(1-2), 58–70.

Johnstone, H. J. H., Yu, J., Elderfield, H., & Schulz, M. (2011). Improving temperature estimates derived from Mg/Ca of planktonic foraminifera using X-ray computed tomography-based dissolution index, XDX. *Paleoceanography*, *26*, PA1215. https://doi.org/10.1029/2009PA001902

Kawahata, H., Nishimura, A., & Gagan, M. K. (2002). Seasonal change in foraminiferal production in the western equatorial Pacific warm pool: Evidence from sediment trap experiments. *Deep Sea Research Part II: Topical Studies in Oceanography*, *49*(13-14), 2783–2800.

Kawahata, H., Suzuki, A., & Ohta, H. (1998). Sinking particles between the equatorial and subarctic regions (0°N–46°N) in the central Pacific. *Geochemical Journal*, *32*(2), 125–133.

Kawahata, H., Suzuki, A., & Ohta, H. (2000). Export fluxes in the Western Pacific Warm Pool. *Deep Sea Research Part I: Oceanographic Research Papers*, *47*(11), 2061–2091.

Keir, R. S. (1980). The dissolution kinetics of biogenic calcium carbonates in seawater. *Geochimica et Cosmochimica Acta*, *44*, 241–252.

Key, R. M., Kozyr, A., Sabine, C. L., Lee, K., Wanninkhof, R., Bullister, J. L., et al. (2004). A global ocean carbon climatology: Results from Global Data Analysis Project (GLODAP). *Global Biogeochemical Cycles*, *18*(4), GB4031. https://doi.org/10.1029/2004GB002247

Klinkhammer, G. P., Haley, B. A., Mix, A. C., Benway, H. M., & Cheseby, M. (2004). Evaluation of automated flow-through time-resolved analysis of foraminifera for Mg/Ca paleothermometry. *Paleoceanography*, *19*, PA4030. https://doi.org/10.1029/2004PA001050

Lammers, L. N., & Mitnick, E. H. (2019). Magnesian calcite solid solution thermodynamics inferred from authigenic deep-sea carbonate. *Geochimica et Cosmochimica Acta*, *248*, 343–355.

Le, J., & Thunell, R. C. (1996). Modelling planktic foraminiferal assemblage changes and application to sea surface temperature estimation in the western equatorial Pacific Ocean. *Marine Micropaleontology*, *28*(3-4), 211–229.

Lohmann, G. P. (2010). A model for variation in the chemistry of planktonic foraminifera due to secondary calcification and selective dissolution. *Paleoceanography*, *10*, 445–457. https://doi.org/10.1029/95PA00059

Martin, W. R., McNichol, A. P., & McCorkle, D. C. (2000). The radiocarbon age of calcite dissolving at the sea floor: Estimates from pore water data. *Geochimica et Cosmochimica Acta*, *64*(8), 1391–1404.

Martin, W. R., & Sayles, F. L. (1996). $CaCO_3$ dissolution in sediments of the Ceara Rise, western equatorial Atlantic. *Geochimica et Cosmochimica Acta*, *60*(2), 243–263.

McClelland, H. L. O., Bruggeman, J., Hermoso, M., & Rickaby, R. E. M. (2017). The origin of carbon isotope vital effects in coccolith calcite. *Nature Communications*, *8*(1), 1–16.

Menard, H. W., & Smith, S. M. (1966). Hypsometry of ocean basin provinces. *Journal of Geophysical Research*, *71*(18), 4305–4325. https://doi.org/10.1029/JZ071i018p04305

Morse, J. W., Mucci, A., & Millero, F. J. (1980). The solubility of calcite and aragonite in seawater of 35 salinity at 25 ^{o}C and atmospheric pressure. *Geochimica et Cosmochimica Acta*, *44*, 85–94.

Mucci, A., & Morse, J. W. (1984). The solubility of calcite in seawater solutions of various magnesium concentration, I_t = 0.697 m at 25 °C and one atmosphere total pressure. *Geochimica et Cosmochimica Acta*, *48*, 815–822.

Naviaux, J. D., Subhas, A. V., Rollins, N. E., Dong, S., Berelson, W. M., & Adkins, J. F. (2019). Temperature dependence of calcite dissolution kinetics in seawater. *Geochimica et Cosmochimica Acta*, *246*, 363–384.

Olsen, A., Key, R. M., van Heuven, S., Lauvset, S. K., Velo, A., Lin, X., et al. (2016). The Global Ocean Data Analysis Project version 2 (GLODAPv2)—An internally consistent data product for the world ocean. *Earth System Science Data*, *8*(2), 297–323.

Olsen, A., Lange, N., Key, R. M., Tanhua, T., Alvarez, M., Becker, S., et al. (2019). GLODAPv2. 2019-an update of GLODAPv2. *Earth System Science Data Discussions*, *11*, 1437–1461. https://doi.org/10.5194/essd-11-1437-2019

Oomori, T., Kaneshima, H., Maezato, Y., & Kitano, Y. (1987). Distribution coefficient of Mg^{2}+ ions between calcite and solution at 10-50 °C. *Marine Chemistry*, *20*(4), 327–336.

Oxburgh, R. (1998). The Holocene preservation history of equatorial Pacific sediments. *Paleoceanography*, *31*, 50–62. https://doi.org/10.1029/97PA02607

Oxburgh, R., & Broecker, W. S. (1993). Pacific carbonate dissolution revisited. *Palaeogeography*, *103*, 31–40.

Parker, F. L., & Berger, W. H. (1971). Faunal and solution patterns of planktonic Foraminifera in surface sediments of the South Pacific. *Deep Sea Research and Oceanographic Abstracts*, *18*(1), 73–107.

Politi, Y., Batchelor, D. R., Zaslansky, P., Chmelka, B. F., Weaver, J. C., Sagi, I., & Addadi, L. (2010). Role of magnesium ion in the stabilization of biogenic amorphous calcium carbonate: A structure-function investigation. *Chemistry of Materials*, *22*(1), 161–166.

Rebotim, A., Voelker, A. H. L., Jonkers, L., Waniek, J. J., Meggers, H., Schiebel, R., et al. (2017). Factors controlling the depth habitat of planktonic foraminifera in the subtropical eastern North Atlantic. *Biogeosciences*, *14*(4), 827–859.

Rongstad, B. L., Marchitto, T. M., & Herguera, J. C. (2017). Understanding the effects of dissolution on the Mg/Ca paleothermometer in planktic foraminifera: Evidence from a novel individual foraminifera method. *Paleoceanography*, *32*, 1386–1402. https://doi.org/10.1002/2017PA003179

Si, W., & Rosenthal, Y. (2019). Reduced continental weathering and marine calcification linked to late Neogene decline in atmospheric CO_2. *Nature Geoscience*, 1–7.

Sigman, D. M., & Boyle, E. A. (2000). Glacial/interglacial variations in atmospheric carbon dioxide. *Nature*, *407*(6806), 859–869.

Sjoberg, E. L., & Rickard, D. (1983). The influence of experimental-design on the rate of calcite dissolution. *Geochimica et Cosmochimica Acta*, *47*(12), 22812285.

Spero, H. J., Bijma, J., Lea, D. W., & Bemis, B. E. (1997). Effect of seawater carbonate concentration on foraminiferal carbon and oxygen isotopes. *Nature*, *390*(6659), 497–500.

Stoll, H. M., Encinar, J. R., Alonso, J. I. G., Rosenthal, Y., Probert, I., & Klaas, C. (2001). A first look at paleotemperature prospects from Mg in coccolith carbonate: Cleaning techniques and culture measurements. *Geochemistry, Geophysics, Geosystems*, *2*(5), 1047. https://doi.org/10.1029/2000GC000144

Subhas, A. V., Rollins, N. E., Berelson, W. M., Dong, S., Erez, J., & Adkins, J. F. (2015). A novel determination of calcite dissolution kinetics in seawater. *Geochimica et Cosmochimica Acta*, *170*(C), 51–68.

Subhas, A. V., Rollins, N. E., Berelson, W. M., Erez, J., Ziveri, P., Langer, G., & Adkins, J. F. (2018). The dissolution behavior of biogenic calcites in seawater and a possible role for magnesium and organic carbon. *Marine Chemistry*, *205*, 100–112.

Sulpis, O., Boudreau, B. P., Mucci, A., Jenkins, C., Trossman, D. S., Arbic, B. K., & Key, R. M. (2018). Current $CaCO_3$ dissolution at the seafloor caused by anthropogenic CO2. *Proceedings of the National Academy of Sciences*, *115*(46), 11,700–11,705.

Sulpis, O., Lix, C., Mucci, A., & Boudreau, B. P. (2017). Calcite dissolution kinetics at the sediment-water interface in natural seawater. *Marine Chemistry*, *195*, 70–83.

Tambutté, S., Holcomb, M., Ferrier-Pages, C., Reynaud, S., Tambutte, E., Zoccola, D., & Allemand, D. (2011). Coral biomineralization: From the gene to the environment. *Journal of Experimental Marine Biology and Ecology*, *408*(1-2), 58–78.

Thunell, R. C. (1976). Optimum indices of calcium carbonate dissolution, in deep- sea sediments. *Geology*, *4*(9), 525–528.

Thunell, R. C., & Honjo, S. (1981). Calcite dissolution and the modification of planktonic foraminiferal assemblages. *Marine Micropaleontology*, *6*(2), 169–182.

Wang, D., Wallace, A. F., De Yoreo, J. J., & Dove, P. M. (2009). Carboxylated molecules regulate magnesium content of amorphous calcium carbonates during calcification. *Proceedings of the National Academy of Sciences*, *106*(51), 21,511–21,516.

Wheatcroft, R. A. (1992). Experimental tests for particle size-dependent bioturbation in the deep ocean. *Limnology and Oceanography*, *37*(1), 90–104.

Young, J. R., & Henriksen, K. (2003). Biomineralization within vesicles: The calcite of coccoliths. *Reviews in Mineralogy and Geochemistry*, *54*(1), 189–215.